Factorization of fragment-production cross sections in relativistic heavy-ion collisions

D. L. Olson* and B. L. Berman
Lawrence Livermore National Laboratory, University of California, Livermore, California 94550

D. E. Greiner, H. H. Heckman, and P. J. Lindstrom
Lawrence Berkeley Laboratory, University of California, Berkeley, California 94720

H. J. Crawford
University of California Space Sciences Laboratory, Berkeley, California 94720

(Received 21 March 1983)

Analysis of the factorizability of several sets of fragment-production cross sections has been performed for ^{12}C, ^{16}O, ^{18}O, and ^{56}Fe projectiles in the 1 to 2 GeV/nucleon energy region for targets ranging from Be to U. The results of this analysis are considered in terms of geometrical concepts. No evidence is found that there is any dependence of fragmentation channel upon the impact parameter. It is found as well that the projectile dependence of the target factors is much less than that predicted by the abrasion-ablation theory, and also is less than that predicted by an excitation-decay model. Nevertheless, it appears that an excitation and decay mechanism is the dominant process in peripheral fragmentation.

[NUCLEAR REACTIONS ^{12}C, ^{16}O, ^{18}O, ^{56}Fe projectiles, Be, C, Al, S, Ti, Cu, Ag, Sn, Ta, W, Pb, U targets. Projectile fragmentation in relativistic heavy-ion collisions. Factorization of nuclear cross sections.]

I. INTRODUCTION

In this paper we investigate the validity of the concept of factorization by the analysis of the data from several measurements of the fragmentation of relativistic heavy ions.[1-3] All of these experiments were performed at the Lawrence Berkeley Laboratory Bevalac. Isotopic fragment-production cross sections were measured both for ^{12}C and ^{16}O projectiles[1] and for ^{18}O projectiles[2] using a magnetic spectrometer to determine the momentum of the fragments and a telescope of Si(Li) detectors to determine their charge. Elemental fragment-production cross sections (only) were measured for ^{56}Fe projectiles,[3] using the same Si(Li) detectors for the charge determination.

The concept of the factorization of fragment-production cross sections originated in the description of processes in high-energy physics.[4] The essential feature of this idea is that at high enough beam energies the branching of the various outgoing particle-production channels is independent of the target. For nuclear fragmentation cross sections, the concepts of "strong" and "weak" factorization have been developed.[5] These concepts can be expressed as

$$\sigma(P,F,T)=\gamma_P^F\gamma_T \tag{1}$$

for strong factorization, and

$$\sigma(P,F,T)=\gamma_P^F\gamma_{PT} \tag{2}$$

for weak factorization, where $\sigma(P,F,T)$ is the nuclear fragmentation cross section for the projectile P incident upon the target T producing the fragment F, γ_P^F is a factor which depends only upon the species of projectile and fragment, γ_{PT} is a factor which depends only upon the species of projectile and target, and γ_T is a factor which is a function solely of the target species.

We test the validity of strong factorization by investigating the deviations from the behavior predicted by the strong-factorization hypothesis for any systematic dependence upon the type of projectile. For the test of weak factorization we investigate the deviations from the behavior predicted by the weak-factorization hypothesis for any systematic dependence upon the fragmentation channel.

II. THEORETICAL MODELS

A. The geometrical model

We obtain a simple picture for nuclear collisions at high energies by considering each nucleus to be a completely absorbing disk and each fragment to be produced from interactions within a certain band of overlap of the two disks. The assumption of totally absorbing disks is made plausible by the fact that the mean free path of nucleons in nuclear matter is only about 1.5 fm (when calculated with the free nucleon-nucleon cross section), and this mean free path is small compared with typical nuclear diameters, which range from about 4.5 fm for ^{12}C to about 13.5 fm for ^{208}Pb.

If the total cross section is given by the area of a disk, then the partial cross sections for producing various fragments of the projectile are just the areas of annular bands of some width. The larger projectile fragments are as-

sumed to come from peripheral interactions between the two nuclei, so that the cross sections for these fragments correspond to bands at the outer edge of the disk. If we sum the measured cross sections for projectile fragments for which the fragment mass is greater than half of the projectile mass and then convert this area to an annulus at the outer edge of the hypothetical absorbing disk, the width of this band is only about 1 fm.[6]

In order to relate these ideas to factorization, we note that the cross section in this case is simply

$$\sigma(P,F,T)=2\pi R(P,T)dR(P,F)\ , \tag{3}$$

so that we can identify γ_{PT} with $2\pi R(P,T)$ and γ_P^F with $dR(P,F)$. In other words, the target factor is proportional to the sum of the radii of the target and projectile nuclei and the fragment factor (which contains the detailed physics) is just the width of the annular band which has an area equal to the measured cross section. For a large target nucleus and a small projectile, γ_{PT} reduces to $\approx 2\pi R(T)$, the circumference of the target nucleus; this is the strong-factorization limit.

However, nuclei do not have perfectly sharp edges; they have a "skin" through which their matter density drops from nearly its central value to nearly zero. The thickness of this skin is about 2 fm. Folding this knowledge into the above model means that the probability of an interaction as a function of impact parameter b (the distance from the center of the absorbing disk) drops essentially from unity to zero over a distance of about 2 fm. We still can retain the picture of annular bands as probability distributions with finite widths, within which the probability peaks at some value of the impact parameter b_0 and falls for smaller and for larger values of b. This is the analog for heavy-ion collisions of the transition charge density for electron scattering; b_0 here corresponds to the transition radius.[7]

Moreover, because of the size of the peripheral fragmentation cross sections, the range of impact parameters must be rather narrow. This means that the target factor cannot be influenced very strongly by the fragmentation channel, and consequently, the weak-factorization condition, Eq. (2), is expected to represent the data adequately.

The assumption here that the target factor is essentially just the sum of the radii of the target and projectile nuclei leads to a quantifiable breakdown of the strong-factorization condition [Eq. (1)]. This seems reasonable within the confines of the present simple idea.

B. The abrasion-ablation theory

The abrasion-ablation theory is essentially a method of computing the probability (as a function of impact parameter) for producing a particular fragment. The abrasion-ablation theory of Hüfner, Schäfer, and Schürmann[8] is constructed around the following simple concept, first introduced by Bowan, Swiatecki, and Tsang.[9] When a relativistic projectile nucleus passes near a target nucleus such that there is an overlap of their matter volumes, the region of the overlap is sheared off (abrasion), leaving a distorted nucleus of smaller mass. This nucleus is now in an excited state by virtue of its distortion, and it deexcites by emitting one or more nucleons (ablation).

In Ref. 8 it is shown, using multiple-scattering theory,[10] that the abrasion cross section for removing n nucleons from the projectile (of mass A_P) is

$$\frac{\partial^2\sigma_n(P,T,\vec{b})}{\partial\vec{b}^{\,2}}=\begin{bmatrix}A_P\\ n\end{bmatrix}[1-P_{PT}(\vec{b})]^n P_{PT}(\vec{b})^{A_P-n}\ , \tag{4}$$

where the impact parameter $\vec{b}$ is the relative position of the projectile with respect to the target in the (x,y) plane for the projectile moving in the z direction. The probability function $P_{PT}(\vec{b})$ is defined by

$$P_{PT}(\vec{b})=\int d^2\vec{t}\,dz\,\rho_P(\vec{t},z)\times\exp\left[-A_T\sigma_{\rm tot}^{\rm NN}\int_{-\infty}^{\infty}\rho_T(\vec{t}+\vec{b},z')dz'\right]\ , \tag{5}$$

where $\sigma_{\rm tot}^{\rm NN}$ is the total nucleon-nucleon cross section and $\rho_i(\vec{t},z)$ is the single-particle density of the projectile ($i=P$) or the target ($i=T$). Since the single-particle densities depend only upon radial distance $[\rho(\vec{t},z)=\rho(r)]$, the probability function $P_{PT}(\vec{b})$ is a function only of the magnitude of the impact parameter $[P_{PT}(\vec{b})=P_{PT}(b)]$. The total abrasion cross section, after integrating over impact parameter, is then

$$\sigma_n(P,T)=\begin{bmatrix}A_P\\ n\end{bmatrix}\int_0^{\infty}2\pi b\,db[1-P_{PT}(b)]^n\times P_{PT}(b)^{A_P-n}\ . \tag{6}$$

Cugnon and Sartor[5] computed the probability function $P_{PT}(b)$ for various cases, and found that its dependence upon target is simply a translation of the impact parameter,

$$P_{PT}(b)=f_P(b-\xi_T) \tag{7}$$

where $f_P(x)$ depends only upon the projectile and ξ_T depends only upon the target. In terms of $f_P(x)$, the abrasion cross section is written as

$$\sigma_n(P,T)=2\pi\begin{bmatrix}A_P\\ n\end{bmatrix}\int_{-\xi_T}^{\infty}dx(x+\xi_T)[1-f_P(x)]^n\times f_P(x)^{A_P-n} \tag{8}$$

and they state that setting the lower limit of integration equal to zero introduces an error of no greater than one percent. By defining N_{nP} (in units of length) to be the normalization constant for the distribution

$$[1-f_P(x)]^n f_P(x)^{A_P-n}$$

and letting $\langle x_{nP}\rangle$ be the value of x averaged over this distribution, the expression for the abrasion cross section can be written as

$$\sigma_n(P,T)=2\pi\begin{bmatrix}A_P\\ n\end{bmatrix}N_{nP}(\langle x_{nP}\rangle+\xi_T)\ , \tag{9}$$

where the term $(\langle x_{nP}\rangle+\xi_T)$ is just the average value of the impact parameter which contributes most strongly to the process for the abrasion of n nucleons. The value of $\langle x_{nP}\rangle$ varies weakly with both n and P. Cugnon and Sartor observe that $\sigma_n(P,T)$ breaks weak factorization by 10 to 15% and strong factorization by a much larger amount.

Bleszynski and Sander[11] noted that the fragmentation cross section is related to the abrasion cross section by

$$\sigma_{\text{calc}}(P,F,T)=\sum_{n=1}^{A_P-A_F}\alpha_n(F,P)\sigma_n(P,T)\ , \tag{10}$$

where $\alpha_n(F,P)$ is the branching ratio for the abraded nucleus of A_P-n nucleons to decay into the final-state fragment F. Including the expression for $\sigma_n(P,T)$, we get

$$\sigma_{\text{calc}}(P,F,T)=2\pi\sum_n\alpha_n(F,P)\begin{bmatrix}A_P\\ n\end{bmatrix}N_{nP}(\langle x_{nP}\rangle+\xi_T) \tag{11}$$

and since the values of $\langle x_{nP}\rangle$ do not vary greatly (for a given P) we can approximately factor the term $(\langle x_{n'}\rangle+\xi_T)$ out of the summation (letting n' denote the dominant n leading to the fragment F) and make the identifications

$$\gamma_P^F=2\pi\sum_n\alpha_n(F,P)\begin{bmatrix}A_P\\ n\end{bmatrix}N_{nP} \tag{12}$$

and

$$\gamma_{PT}=\langle x_{n'P}\rangle+\xi_T\ . \tag{13}$$

According to Ref. 8, the excitation energies of the abraded nuclei are low enough so that there is typically only one or two particles emitted in the ablation stage, which corresponds to one or two terms in the summation in Eq. (11).

We can see that the target factor of Eq. (13) corresponds to the average impact parameter for a particular fragmentation channel (n'). A deviation from weak factorization can be taken to mean that there is a dependence of the fragmentation channel upon the impact parameter or, conversely, if weak factorization holds exactly then there is no impact parameter dependence within the fragmentation channel. We note that a lack of deviation from weak factorization is contrary to the basic premise of the abrasion stage of the abrasion-ablation theory.

C. The excitation-decay model

We have derived an alternative description of peripheral fragmenation through the use of the theory of nucleus-nucleus total reaction cross sections as formulated by Karol.[12] The following discussion [Eqs. (14)—(19)] summarizes the result of Karol's work and is used as the basis of our model. The total reaction cross section is computed as

$$\sigma_R=2\pi\int_0^\infty[1-T(b)]b\,db\ , \tag{14}$$

where $T(b)$ is the transmission probability, i.e., the probability that the projectile will not interact with the target at impact parameter b. The reaction cross section is

$$\sigma_R=10\pi(a_T^2+a_P^2)[E_1(\chi)+\ln(\chi)+\gamma]\ , \tag{15}$$

where $E_1(\chi)$ is the exponential integral and γ is Euler's constant. The parameters a_T and a_P are given by

$$a_i^2=\frac{4c_it_i+t_i^2}{k}\ , \tag{16}$$

where c_i is the half-central-density radius, t_i is the skin thickness, and $k=4\ln 5$. χ is given by the expression

$$\chi=\frac{\pi^2\bar{\sigma}(E)\rho_T(0)\rho_P(0)a_T^3a_P^3}{10(a_T^2+a_P^2)}\ , \tag{17}$$

where $\bar{\sigma}(E)$ is the average energy-dependent nucleon-nucleon cross section and $\rho_i(0)$ is given by

$$\rho_i(0)=\tfrac{1}{2}\rho_{oi}\exp(c_i/a_i)^2\ , \tag{18}$$

where

$$\rho_{oi}=\frac{3A_i}{4\pi c_i^3[1+(\pi^2t_i^2/19.36c_i^2)]}\ . \tag{19}$$

This reaction cross section is related to peripheral fragmentation cross sections in the following way. Consider reactions in which there is a single quasielastic nucleon-nucleon collision. In this case, fragmentation resulting in the projectile losing more than one nucleon is an excitation and decay process where the scattered nucleon must impart sufficient energy to the projectile in order to allow the latter to decay into the various fragmentation channels. At this point we make the simplifying assumption that the excitation energy ϵ of the projectile is just the kinetic energy of the struck nucleon in the projectile.

In order to consider the excitation-energy dependence of the peripheral-fragmentation cross section, we differentiate Eq. (15) with respect to ϵ,

$$\frac{\partial\sigma_R}{\partial\epsilon}=10\pi(a_T^2+a_P^2)\left[\frac{\partial E_1(\chi)}{\partial\epsilon}+\frac{\partial\ln(\chi)}{\partial\epsilon}\right]\ . \tag{20}$$

For a typical case ($P=^{12}$C, $T=^{56}$Fe, and $\bar{\sigma}\approx 10$ to 40 mb), we have $\chi\geq 4.5$ and $E_1(\chi)\leq 2\times10^{-3}$, so that $\partial E_1(\chi)/\partial\epsilon$ is negligible. Also, the only factor in χ which depends upon ϵ is $\bar{\sigma}$, so that $\partial\ln(\chi)/\partial\epsilon=\partial\ln\bar{\sigma}/\partial\epsilon$. Clearly, the relative branching ratios for different fragmentation channels will depend upon ϵ. We can write the excitation-energy-dependent fragment-production cross section as

$$\frac{\partial\sigma(P,F,T)}{\partial\epsilon}=10\pi(a_T^2+a_P^2)\frac{\partial\ln\bar{\sigma}}{\partial\epsilon}\alpha_P^F(\epsilon)\ . \tag{21}$$

A calculation of the branching ratios $\alpha_P^F(\epsilon)$ would involve the probabilities for particle emission from a nucleus P with excitation energy ϵ. This is not our goal here; rather, we note that $\alpha_P^F(\epsilon)$ does not depend upon the type of target T. From Eq. (21) we obtain the total fragment-production cross section by integrating over ϵ

$$\sigma(P,F,T)=10\pi(a_T^2+a_P^2)\int_{\epsilon_F}^{\epsilon_P}\frac{\partial\ln\bar{\sigma}}{\partial\epsilon}\alpha_P^F(\epsilon)d\epsilon\ , \tag{22}$$

where ϵ_F is the energy threshold for fragment F and ϵ_P is the projectile energy per nucleon. This integral has no

TABLE I. Cross sections (in mb) for ^{16}O projectiles.[a] An asterisk indicates an EMD fragment.

	Target						
Fragment	H	Be	C	Al	Cu	Ag	Pb
$^{15}O^*$	(27.3 ± 2.6)	43.0 ± 2.2	42.9 ± 2.3		(74.0 ± 7.8)	(99 ±13)	(135 ± 22)
^{14}O	(0.75± 0.12)	1.60± 0.10	1.67± 0.12		2.14± 0.42	2.20± 0.58	(2.8 ± 1.5)
^{13}O	(0.17± 0.03)	0.32± 0.04	0.22± 0.03		0.52± 0.17		
^{16}N	(0.02[b])	(0.05± 0.02)	0.13± 0.02	0.10±0.03		(0.39± 0.15)	(0.06[b])
$^{15}N^*$	(34.3 ± 3.3)	54.1 ± 2.7	54.2 ± 2.9	66.0 ±4.3	(98.2 ± 9.6)	(121 ±15)	(202 ± 26)
^{14}N	(31.0 ± 3.3)	49.5 ± 4.0	41.8 ± 3.3		72 ±14	68 ±23	71 ± 22
^{13}N	(4.49± 0.46)	8.01± 0.40	8.06± 0.42		14.7 ± 1.6	18.6 ± 2.2	17.0 ± 3.2
^{12}N	(0.40± 0.07)	0.66± 0.05	0.73± 0.07		(0.42± 0.18)	1.11± 0.34	
^{15}C	(0.02± 0.01)	0.05± 0.01	0.04± 0.01		(0.11± 0.08)		
^{14}C	(3.69± 0.38)	5.21± 0.30	4.71± 0.31	6.29±0.46	7.76± 0.92	7.5 ± 1.3	12.3 ± 2.2
^{13}C	(17.8 ± 1.7)	28.6 ± 1.4	27.7 ± 1.4	31.4 ±2.0	35.8 ± 3.7	39.4 ± 5.1	45.4 ± 8.3
^{12}C	(32.3 ± 4.8)	60.8 ± 4.9	65.1 ± 5.2		92 ±14	104 ±18	126 ± 25
^{11}C	(11.0 ± 1.1)	21.0 ± 1.1	18.46± 0.92		27.0 ± 2.6	37.8 ± 3.8	36.9 ± 5.7
^{10}C	(1.83± 0.21)	2.81± 0.17	2.51± 0.16		4.45± 0.52	4.2 ± 1.2	7.2 ± 1.4
^{9}C	(0.21± 0.08)		0.41± 0.09				
^{13}B	(0.31± 0.05)	0.50± 0.04	0.44± 0.05		0.82± 0.17	(0.65± 0.28)	(0.70± 0.44)
^{12}B	(1.45± 0.17)	2.75± 0.15	2.44± 0.15	3.61±0.24	2.98± 0.38	4.04± 0.58	3.98± 0.75
^{11}B	(15.4 ± 1.5)	27.5 ± 1.4	26.0 ± 1.3	31.0 ±1.6	35.9 ± 2.9	43.6 ± 3.9	52.9 ± 5.9
^{10}B	(8.9 ± 1.7)	19.2 ± 1.5	20.3 ± 1.6		35.2 ± 5.5	26.6 ± 6.3	35 ± 11
^{8}B	(0.58± 0.08)	1.53± 0.12	1.38± 0.13		1.38± 0.34		
^{12}Be	(0.04± 0.02)		0.03± 0.02				
^{11}Be	(0.08± 0.03)		0.19± 0.03		(0.30± 0.13)		
^{10}Be	(2.05± 0.31)	3.92± 0.27	3.98± 0.30		6.51± 0.86	5.65± 0.77	6.8 ± 1.1
^{9}Be	(4.17± 0.55)	9.79± 0.50	9.06± 0.51	11.22±0.68	12.3 ± 1.1	13.8 ± 1.5	15.3 ± 2.1
^{7}Be	(10.1 ± 1.2)	22.0 ± 1.1	22.3 ± 1.1		32.0 ± 2.5	36.4 ± 3.2	43.3 ± 6.4
^{9}Li	(0.34± 0.08)		0.51± 0.07				
^{8}Li	(0.73± 0.17)		2.50± 0.18		3.63± 0.47		
^{7}Li	(11.1 ± 1.3)	27.0 ± 1.4	26.3 ± 1.3	34.8 ±1.8	38.7 ± 2.9	39.8 ± 3.5	39.7 ± 4.3
^{6}Li	(13.3 ± 2.4)	33.5 ± 2.7	35.9 ± 2.9		61.2 ± 7.9	49.4 ± 8.5	56 ± 13
^{6}He	(0.73± 0.20)		2.00± 0.21				
^{4}He	(221 ±20)	501 ±45	474 ±42		748 ±80	825 ±90	882 ±104
^{3}He	(50.2 ± 5.7)	152.4 ± 8.5	136.0 ± 7.6				
^{3}H	(55 ±11)		(151 ±11)				
^{2}H	(152 ±23)	(417 ±37)	(406 ±36)		(682 ±72)	(752 ±97)	(945 ±154)
$^{1}H^c$	(37.2 ± 6.8)		(96.5 ± 6.2)				

[a]Parentheses indicate the cross sections which were not included in the factorization analysis.

[b]Estimated to within a factor of 2.

[c]Produced within 12.5 mrad of the incident beam direction.

TABLE II. Cross sections (in mb) for ^{12}C projectiles at 2.1 GeV/nucleon.[a] An asterisk indicates an EMD fragment.

Fragment	Target H	Be	C	Al	Cu	Ag	Pb
^{12}N	(0.03± 0.01)	(0.06± 0.01)	(0.08± 0.01)			(0.24± 0.09)	
$^{11}C^*$	(26.1 ± 2.4)	46.7 ± 2.3	46.5 ± 2.3	59.5 ± 3.1	(81.4 ± 6.3)	(101.9 ± 9.6)	(145 ± 17)
^{10}C	(2.38± 0.24)	4.20± 0.21	4.11± 0.22	4.99± 0.34	5.38 ± 0.55	7.03± 0.88	7.8 ± 1.5
^{9}C	(0.38± 0.07)	0.54± 0.06	0.54± 0.07	0.50± 0.09	0.52± 0.17	(0.53± 0.27)	(1.56± 0.57)
^{12}B	(0.06± 0.01)	0.14± 0.02	0.10± 0.01	0.14± 0.03	(0.12± 0.08)		(0.11[c])
$^{11}B^*$	(30.9 ± 3.4)	53.2 ± 2.9	53.8 ± 2.7	65.2 ± 4.8	(84.8 ± 9.0)	(109 ±13)	(155 ± 23)
^{10}B	(16.9 ± 3.0)	31.1 ± 2.6	35.1 ± 3.4	36.4 ± 4.8	43.7 ± 9.8	65 ±17	74 ± 25
^{8}B	(0.47± 0.11)	1.48± 0.09	1.72± 0.13	1.76± 0.14	1.85± 0.33	1.96± 0.40	3.69± 0.76
^{11}Be		(0.02± 0.01)					
^{10}Be	(3.42± 0.35)	5.97± 0.31	5.81± 0.29	7.02± 0.40	8.57± 0.70	8.81± 0.91	10.0 ± 1.4
^{9}Be	(5.92± 0.54)	10.98± 0.55	10.63± 0.53	12.74± 0.71	16.1 ± 1.3	18.6 ± 1.7	22.5 ± 2.6
^{7}Be	(9.5 ± 1.0)	18.91± 0.95	18.61± 0.93	25.8 ± 1.3	33.7 ± 2.3	41.2 ± 3.3	47.9 ± 4.9
^{9}Li	(0.41± 0.08)	0.92± 0.08	0.85± 0.08	0.88± 0.12	1.38± 0.36	1.20± 0.33	(1.43± 0.53)
^{8}Li	(1.13± 0.16)	2.52± 0.16	2.18± 0.15	2.79± 0.23	3.89± 0.47	3.27± 0.53	3.40± 0.82
^{7}Li	(11.0 ± 1.0)	22.8 ± 1.1	21.5 ± 1.1	27.3 ± 1.4	31.9 ± 2.3	40.3 ± 3.3	45.9 ± 4.6
^{6}Li	(13.9 ± 1.5)	33.1 ± 2.7	30.0 ± 2.4	36.3 ± 2.9	47.3 ± 4.5	46.1 ± 5.6	60.0 ± 8.5
^{6}He	(0.91± 0.21)	2.54± 0.25	2.21± 0.22	2.82± 0.27	3.21± 0.47	3.5 ± 1.1	4.2 ± 1.1
^{4}He	(171 ±15)	383 ±34	373 ±33	451 ±40	553 ±59	616 ±67	728 ± 85
^{3}He	(51.5 ± 4.5)	127.9 ± 7.2	124.9 ± 7.0	152.2 ± 9.4	192 ±13	227 ±16	264 ± 22
^{3}H	(53 ±10)	(134 ±10)	(129 ±11)	(158 ±14)	(198 ±24)	(237 ±32)	(321 ± 52)
^{2}H	(105 ±15)	(329 ±30)	(314 ±28)	(411 ±37)	(543 ±58)	(690 ±78)	(715 ±124)
$^{1}H^b$	(24.1 ± 4.1)	(71.7 ± 4.2)	(70.0 ± 4.2)	(86.3 ± 5.7)	(112.0 ± 8.9)	(131 ±12)	(171 ± 18)

[a]Parentheses indicate which cross sections were not included in the factorization analysis.
[b]Produced within 12.5 mrad of the incident beam direction.
[c]Estimated to within a factor of 2.

TABLE III. Cross sections (in mb) for ^{12}C projectiles at 1.05 GeV/nucleon.[a] An asterisk indicates an EMD fragment.

Fragment	Target H	Be	C	Al	Cu	Ag	Pb
^{12}N	(0.05[b])	(0.02± 0.01)	(0.05[b])	(0.07± 0.03)			
$^{11}C^*$	(25.0 ± 3.0)	44.7 ± 2.6	44.7 ± 2.8	57.8 ± 3.9	(78.1 ± 8.1)	(98 ±13)	(128 ± 22)
^{10}C	(2.52± 0.28)	4.02± 0.23	4.44±0.24	5.06± 0.37	7.53± 0.70	7.7 ± 1.0	10.9 ± 1.7
^{9}C	(0.28± 0.06)	0.42± 0.05	0.48± 0.06	0.60± 0.10	0.67± 0.18	1.19± 0.30	
^{12}B	(0.05± 0.01)	0.09± 0.02	0.10± 0.01	0.18± 0.05	0.15± 0.05		(0.23[b])
$^{11}B^*$	(29.3 ± 2.7)	50.7 ± 3.2	48.6 ± 2.4	64.5 ± 5.3	(80.1 ± 7.9)	(110 ±15)	(149 ±25)
^{10}B	(20.2 ± 2.5)	28.8 ± 2.3	27.9 ± 2.2	30.4 ± 3.5	36.4 ± 9.9	43 ±12	(51 ± 18)
^{8}B	(0.60± 0.09)	1.55± 0.08	1.43± 0.10	1.73± 0.16	2.29± 0.32	1.78± 0.38	2.70± 0.68
^{11}Be		(0.02± 0.01)					
^{10}Be	(3.41± 0.54)	5.08± 0.30	5.34± 0.29	6.49± 0.48	7.69± 0.61	8.4 ± 1.2	10.9 ± 1.8
^{9}Be	(5.13± 0.54)	11.60± 0.70	10.70± 0.50	13.90± 0.90	14.3 ± 1.2	23.7 ± 2.7	22.2 ± 3.7
^{7}Be	(8.45± 0.81)	17.80± 0.90	18.60± 0.90	19.9 ± 1.1	25.0 ± 1.9	21.6 ± 2.7	37.8 ± 4.7
^{9}Li	(0.40± 0.09)	0.75± 0.08	0.87± 0.01	0.82± 0.16	1.05± 0.38	(1.15± 0.49)	(1.76± 0.81)
^{8}Li	(0.77± 0.14)	2.36± 0.14	2.40± 0.18	2.87± 0.27	3.99± 0.70	(2.8 ± 1.2)	4.9 ± 1.6
^{7}Li	(10.40± 0.80)	23.4 ± 1.2	21.5 ± 1.1	28.5 ± 1.4	32.6 ± 1.9	42.1 ± 3.4	45.2 ± 4.8
^{6}Li	(11.5 ± 2.2)	24.8 ± 2.0	27.1 ± 2.2	24.9 ± 2.9	33.1 ± 6.0	38.1 ± 7.6	51 ± 13
^{6}He	(0.94± 0.19)	2.09± 0.17	1.83± 0.19	2.00± 0.29	3.01± 0.68	(3.6 ± 1.4)	(7.3 ± 2.7)
^{4}He	(185 ±19)	422 ±38	404 ±36	488 ±44	568 ±61	727 ±79	749 ±113
^{3}He	(46.4 ± 5.1)	134 ± 7	135 ± 8	161 ± 9	209 ±14	237 ±17	321 ± 26
^{3}H		(124 ± 7)	(118 ± 7)	(149 ± 9)	(219 ±19)		
^{2}H	(125 ±16)	(301 ±27)	(292 ±26)	(413 ±37)	(485 ±52)	(698 ±82)	(823 ±145)
$^{1}H^c$	(7.0 ± 1.5)	(20.2 ± 1.4)	(18.8 ± 1.6)	(24.6 ± 2.1)	(26.4 ± 3.7)	(35.9 ± 5.2)	(48.7 ± 8.2)

[a]Parentheses indicate the cross sections which were not included in the factorization analysis.

[b]Estimated to within a factor of 2.

[c]Produced within 12.5 mrad of the incident beam direction.

dependence upon the type of target, so that we can make the identifications

$$\gamma_P^F = K 10\pi \int_{\epsilon_F}^{\epsilon_P} \frac{\partial \ln \bar{\sigma}}{\partial \epsilon} \alpha_P^F(\epsilon) d\epsilon \tag{23}$$

and

$$\gamma_{PT} = K^{-1}(\alpha_P^2 + \alpha_T^2) , \tag{24}$$

where K (in units of length) is a relative normalization constant. Since the skin thickness t_i is approximately constant for all nuclei the parameter a_i^2 is essentially a measure of the radius of the ith nucleus, so that γ_{PT} is proportional to the sum of the radii of the target and projectile nuclei plus a constant.

We see that weak factorization is predicted exactly by this model and that strong factorization is predicted to be broken by the dependence of the target factor upon the sum of the radii of the target and projectile nuclei. Essentially, this model predicts that the size of the fragment does not depend upon the amount of overlap of the target and projectile nuclei, which implies in turn that the excitation spectrum of the projectile-fragment system must extend to energies sufficiently high to produce the small fragments.

III. RESULTS AND DISCUSSION

A. Empirical determinations of fragment and target factors

The data from the ^{18}O experiment[2] and from the earlier experiment[1] with ^{12}C and ^{16}O projectiles were analyzed in order to determine the factors γ_p^F and γ_{PT}. These factors result from minimizing χ^2 in the expression

$$\chi^2 = \sum_P \sum_F \sum_T \frac{[\sigma(P,F,T) - \gamma_P^F \gamma_{PT}]^2}{[\delta\sigma(P,F,T)]^2} , \tag{25}$$

where $\delta\sigma(P,F,T)$ is the experimental uncertainty in the measured fragment-production cross section $\sigma(P,F,T)$.

This analysis was performed with sets of cross sections for ^{18}O projectiles at 1.7 GeV/nucleon, ^{16}O projectiles at 2.1 GeV/nucleon, ^{12}C projectiles at 2.1 GeV/nucleon, and ^{12}C projectiles at 1.05 GeV/nucleon. The cross sections used in our analysis for the ^{18}O projectiles are those listed in Ref. 2, with the exception of those for heavy targets and fragmentation channels with significant electromagnetic dissociation (EMD) and those for the ^{6}Li fragmentation channel, the latter because of systematic uncertainties which are discussed in Ref. 2. The cross sections we used for the ^{16}O data and the two ^{12}C data sets are listed without parentheses in Tables I–III. These include all of the measured cross sections except those for the EMD fragmentation channels with heavy targets, those reactions with hydrogen targets or hydrogen fragments, and those where the experimental uncertainty is greater than 30% of the measured value for the cross section, all of which are listed with parentheses.

It should be noted that the hydrogen-fragment and hydrogen-target data do not fit well within the factorization hypotheses, but this is a special issue, and thus a discussion of the behavior of the hydrogen data is beyond the scope of the present paper.

The resulting fragment and target factors are listed in Tables IV–VII, with the normalization that $\gamma_{PT}=1$ for $T=$Be. In general, the units of the target and fragment

TABLE IV. Fragment and target factors for ^{18}O projectiles.

Fragment	γ_P^F	Target	γ_{PT}
^{18}F	0.520±0.049	U	2.052±0.030
^{17}O	45.86 ±0.93	Pb	1.990±0.033
^{16}O	32.06 ±0.70	W	1.90 ±0.10
^{17}N	27.89 ±0.40	Sn	1.92 ±0.11
^{16}N	21.12 ±0.88	Cu	1.604±0.096
^{15}N	53.74 ±0.74	Ti	1.468±0.025
^{14}N	12.52 ±0.22	Al	1.264±0.012
^{15}C	3.670±0.086	C	1.022±0.010
^{14}C	28.49 ±0.52	Be	1.000±0.009
^{13}C	37.10 ±0.68		
^{12}C	28.65 ±0.37		
^{12}B	8.24 ±0.19		
^{10}B	8.65 ±0.17		
^{10}Be	10.35 ±0.14		
^{7}Li	23.09 ±0.44		

TABLE V. Fragment and target factors for ^{16}O projectiles.

Fragment	γ_P^F	Target	γ_{PT}
^{15}O	43.8 ± 1.5	Pb	1.731±0.067
^{14}O	1.638± 0.071	Ag	1.557±0.047
^{13}O	0.268± 0.023	Cu	1.402±0.034
^{16}N	0.114± 0.015	Al	1.210±0.027
^{15}N	55.1 ± 1.7	C	0.958±0.012
^{14}N	46.4 ± 2.4	Be	1.000±0.012
^{13}N	8.52 ± 0.27		
^{12}N	0.693± 0.039		
^{15}C	0.046± 0.007		
^{14}C	5.16 ± 0.17		
^{13}C	27.54 ± 0.76		
^{12}C	64.7 ± 3.1		
^{11}C	20.27 ± 0.60		
^{10}C	2.78 ± 0.11		
^{9}C	0.428± 0.090		
^{13}B	0.491± 0.030		
^{12}B	2.645± 0.082		
^{11}B	26.86 ± 0.66		
^{10}B	20.2 ± 1.0		
^{8}B	1.430± 0.081		
^{11}Be	0.198± 0.030		
^{10}Be	4.02 ± 0.17		
^{9}Be	9.35 ± 0.26		
^{7}Be	22.77 ± 0.65		
^{9}Li	0.532± 0.070		
^{8}Li	2.61 ± 0.16		
^{7}Li	27.11 ± 0.66		
^{6}Li	35.5 ± 1.7		
^{6}He	2.09 ± 0.21		
^{4}He	510 ±22		
^{3}He	146.8 ± 5.6		

TABLE VI. Fragment and target factors for ^{12}C projectiles at 2.1 GeV/nucleon.

Fragment	γ_P^F	Target	γ_{PT}
^{11}C	48.0 ± 1.2	Pb	1.983±0.067
^{10}C	4.15 ± 0.11	Ag	1.669±0.046
^{9}C	0.496± 0.033	Cu	1.460±0.034
^{12}B	0.112± 0.008	Al	1.193±0.018
^{11}B	54.4 ± 1.6	C	0.971±0.013
^{10}B	32.4 ± 1.5	Be	1.000±0.013
^{8}B	1.510± 0.051		
^{10}Be	5.84 ± 0.14		
^{9}Be	10.94 ± 0.25		
^{7}Be	20.59 ± 0.45		
^{9}Li	0.854± 0.042		
^{8}Li	2.330± 0.076		
^{7}Li	22.65 ± 0.50		
^{6}Li	31.0 ± 1.0		
^{6}He	2.34 ± 0.11		
^{4}He	378 ±13		
^{3}He	130.1 ± 3.0		

factors are arbitrary except that the product must be an area. We adopt the convention that the units of each are length and that the product yields area in mb. We note that the factors for ^{12}C projectiles at 2.1 GeV nucleon are not significantly different from those for 1.05 GeV/nucleon. In addition, the factors for ^{56}Fe projectiles from Ref. 3 (except for Mn fragments) are listed in Table VIII, again with $\gamma_{PT}=1$ for $T=B$. The fragmentation channels in this case are for elements (and not for isotopes).

B. Strong factorization

The validity of strong factorization was predicted by Cugnon and Sartor[5] to be violated to such an extent so as not to be a useful concept. Specifically, we must determine the systematic projectile dependence of the target factor. The target factors for each of the tabulated data sets are plotted in Fig. 1. The data points for ^{12}C shown in Fig. 1 are the average values of the target factors from the two experimental energies. The factors for each projectile have been normalized such that the average value for the Be and C targets is unity. The curves shown are fits to each set of target factors with a function of the form

TABLE VII. Fragment and target factors for ^{12}C projectiles at 1.05 GeV/nucleon.

Fragment	γ_P^F	Target	γ_{PT}
^{11}C	45.7 ± 1.5	Pb	2.112±0.088
^{10}C	4.35 ± 0.13	Ag	1.664±0.057
^{9}C	0.465± 0.031	Cu	1.451±0.037
^{12}B	0.101± 0.008	Al	1.194±0.022
^{11}B	50.2 ± 1.6	C	0.996±0.015
^{10}B	27.6 ± 1.3	Be	1.000±0.015
^{8}B	1.472± 0.049		
^{10}Be	5.26 ± 0.15		
^{9}Be	11.08 ± 0.30		
^{7}Be	17.30 ± 0.43		
^{9}Li	0.778± 0.053		
^{8}Li	2.398± 0.090		
^{7}Li	22.91 ± 0.52		
^{6}Li	24.3 ± 1.1		
^{6}He	1.92 ± 0.10		
^{4}He	406 ±16		
^{3}He	138.3 ± 3.3		

TABLE VIII. Fragment and target factors for ^{56}Fe projectiles.[a]

Fragment[b]	γ_P^F	Target	γ_{PT}
Cr	117.2±3.1	U	1.76±0.09
V	89.2±2.9	Pb	1.72±0.10
Ti	79.1±2.9	Ta	1.74±0.09
Sc	72.0±2.7	Ag	1.52±0.07
Ca	73.0±2.7	Cu	1.36±0.07
K	57.5±2.5	S	1.05±0.07
Ar	55.6±2.5	C	0.99±0.05
		Be	1.00±0.04
		Li	0.92±0.02
		H	0.73±0.05

[a]Taken from Ref. 3.
[b]Fragments identified only by element (and not by isotope).

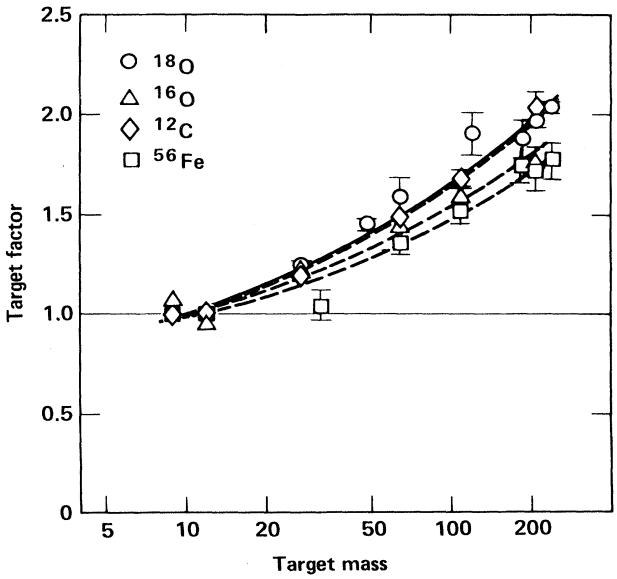

FIG. 1. Normalized target factors γ_{PT} for the projectiles ^{12}C, ^{16}O, ^{18}O, and ^{56}Fe. The factors for each projectile are normalized such that the average value for Be and C targets is unity. The curves are the results of fitting the data with a function of the form

$$\gamma_{PT}=g(A_T^{1/3}+A_P^{1/3}-\delta)$$

where g and δ are fitting parameters (see Table IX). The solid curve corresponds to the ^{18}O data, the short-dashed curve to the ^{12}C data, the medium-dashed curve to the ^{16}O data, and the long-dashed curve to the ^{56}Fe data.

TABLE IX. Parameters from strong-factorization analysis.

Parameter	Projectile ^{18}O	^{16}O	^{12}C	^{56}Fe
g[a]	0.265±0.002	0.221±0.004	0.261±0.003	0.202±0.003
δ	0.09 ±0.04	0.16 ±0.10	0.65 ±0.06	1.13 ±0.11
γ_{PT}	1.999±0.019	1.830±0.043	1.975±0.031	1.740±0.036
From curve[b] ratio with respect to ^{56}Fe	1.149±0.023	1.052±0.031	1.135±0.029	1.000

[a]The units of g are the same as those for γ_{PT}.
[b]For $A_T=208$.

$$\gamma_{PT}=g(A_T^{1/3}+A_P^{1/3}-\delta)\ ,$$

where g and δ are adjustable parameters. The resulting values for g and δ are listed in Table IX. Our geometrical model constitutes the basis for this parametrization of the target factors: δ is a relative measure of the overlap of the target and projectile nuclei which contributes to peripheral fragmentation.

The test of strong factorization hinges upon a comparison of the target factors for the different projectiles. Consider the values of the fitted curves for $A_T=208$ (T=Pb). These values are listed in Table IX, along with the ratio of the value for each of the light projectiles to that for ^{56}Fe. In order to compare with the abrasion-ablation theory, we compute the target factors for the projectiles ^{12}C and ^{56}Fe with a Pb target by estimating the values for $\langle x_{nP}\rangle$ and ξ_T with the normalization appropriate to Fig. 1. This ratio is 1.29, which is to be compared to the value 1.14±0.03 from the data. Computing this ratio by the use of our excitation-decay model [Eq. (24)], with values of c_i and t_i obtained from Ref. 13, we produce the value 1.21, which also is larger than that for the data. If the data were to exhibit precisely the behavior of strong factorization, the value of this ratio would be unity. This is clearly not the case. However, it also is clear that the data do not exhibit as great a dependence upon the projectile as that predicted by either the abrasion-ablation theory or our excitation-decay model.

Both of the theoretical models considered here predict that the values of target factors for Pb targets decrease monotonically with increasing size of the projectile. This behavior also is not exhibited by the data, although the variations between the different sets of data in Fig. 1 are possibly the result of systematic errors and are not conclusively physical in nature. However, the fact that the ^{56}Fe data are consistently lower than those for the smaller projectiles is in agreement with the trend of the theoretical models.

Even though we cannot make a definitive determination of the extent to which the data deviate from the strong-factorization limit, the data do indicate that strong factorization is broken, but to a significantly lesser extent than that predicted by the models.

C. Weak factorization

In order to see how well the factors γ_P^F and γ_{PT} (Tables IV–VII) fit the measured cross sections, we compute the ratio

$$r(P,F,T)=\gamma_P^F\gamma_{PT}/\sigma(P,F,T) \tag{26}$$

for each of the cross sections $\sigma(P,F,T)$. First, we determine the mean value

$$\bar{r}=\sum_{PFT} r/N_\sigma$$

and the width

$$\Gamma_r=\left[\sum_{PFT}(r-\bar{r})^2/N_\sigma\right]^{1/2}$$

for each set of cross sections (N_σ is number of cross sections in the sum). Table X shows the results of this analysis. That the values for $\bar{r}$ are nearly equal to unity is merely a verification that the γ_P^F and γ_{PT} were computed correctly. That the values for $\bar{r}$ are not *exactly* equal to unity results from the fact that the weighting factors are the inverse squares of the error bars; i.e., the cross sections are not weighted uniformly. The values for Γ_r for ^{12}C and ^{16}O projectiles are considerably larger than that for ^{18}O projectiles. However, in consideration of the large χ^2 for the ^{18}O case, it is apparent that the different value for

TABLE X. Parameters from weak-factorization analysis.

Projectile	N_σ	N_{df}[a]	$\bar{r}$	Γ_r	χ^2
^{18}O	77	53	1.001	0.039	225[b]
^{16}O	118	81	1.016	0.118	75
^{12}C[c]	90	67	1.000	0.097	52
^{12}C[d]	86	63	1.011	0.115	55

[a]N_{df} is the number of degrees of freedom.
[b]Results from weighting with statistical uncertainties only; see text for a discussion of systematic uncertainties and the significance of χ^2.
[c]2.1 GeV/nucleon.
[d]1.05 GeV/nucleon.

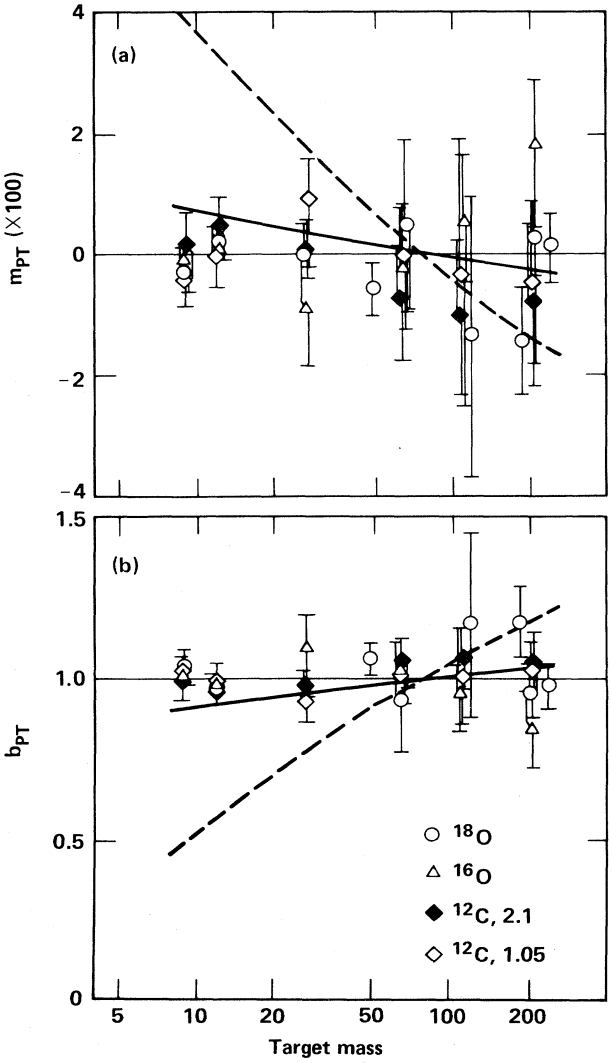

FIG. 2. Comparison of the measured values for (a) m_{PT} and (b) b_{PT} with those expected from the abrasion-ablation theory, for ^{18}O, ^{16}O, ^{12}C at 2.1 GeV/nucleon, and ^{12}C at 1.05 GeV/nucleon projectiles (see the text for the derivation of these values). The dashed curves correspond to the predictions of the abrasion-ablation theory. The solid curves result from the assumption that the target factor is the sum of the radii of the target and *fragment* nuclei (see the text).

Γ_r results from nonstatistical experimental uncertainties which are not included in the weighting function. The systematic uncertainties for the ^{18}O cross sections are approximately 5% of the measured values of these cross sections. If this 5% were included in the factorization analysis, the ^{18}O data would be perfectly consistent with the weak-factorization condition [Eq. (2)].

Next, we investigate these values for r in order to determine whether and to what extent there is any systematic dependence either upon A_F or upon A_T. In this analysis, the values for r are fitted with the linear function

$$r(P,F,T)=m_{PT}A_F+b_{PT}\ , \tag{27}$$

thus generating values for the parameters m_{PT} and b_{PT}. According to the abrasion-ablation theory, there should be a systematic dependence of m_{PT} (or equivalently, of b_{PT}) upon A_T. Figures 2(a) and (b) show the resulting values for m_{PT} and for b_{PT}, respectively. As a result of the procedure for calculating the values for r, the parameters m_{PT} and b_{PT} are not independent; they provide two views of the same information. Note that a zero value for m_{PT} (or equivalently, a value of unity for b_{PT}) means that the values for r (a measure of the deviation from weak-factorization behavior) have no dependence upon the fragmentation channel.

The deviation from weak factorization predicted by the abrasion-ablation theory results from the fact that the target factor is not only a function of the target and projectile, but also depends somewhat upon the fragmentation channel, through the dependence of $\langle x_{nP}\rangle$ upon n and P. It is possible to compute the systematic behavior of this predicted deviation from weak factorization and to obtain an estimate of its magnitude. For this, values of $\langle x_{nP}\rangle+\xi_T$ are used in place of those for $\sigma(P,F,T)$ in the analysis described above. The set of values for $\langle x_{nP}\rangle$ and ξ_T used for this is given in Table XI, and was chosen to be a representative sample for ^{18}O projectiles. It should be noted that this sample spans a somewhat smaller range of target and fragment sizes than the full ^{18}O data set in order to provide a conservative estimate for the predicted deviation from weak factorization.

The systematic behavior of the values for $r(F,T)$ which result from this analysis, shown in Table XII, is such that r(heavy,light) and r(light,heavy) are greater than unity while r(light,light) and r(heavy,heavy) are less than unity. The values for m_{PT} and b_{PT} which were determined from this analysis are plotted as the dashed curves in Figs. 2(a) and (b). It is readily apparent that the data show no systematic dependence upon the fragmentation channel, in striking disagreement with the abrasion-ablation theory.

Alternatively, one can consider another geometrical model in which there is a smaller but nonzero deviation from weak factorization. In this model we include explicitly the overlap of the emitted larger fragment and the target by assuming that the target factor is the sum of the radii of the target and *fragment* nuclei:

$$\gamma_{PT}=r_0(A_T^{1/3}+A_F^{1/3})\ .$$

TABLE XI. Values for $\langle x_{nP}\rangle$ and ξ_T for ^{18}O projectiles.

n	A_F[a]	$\langle x_{nP}\rangle$	Target	ξ_T
1	15	7.8	C	−2.3
3	13	6.8	Al	−1.3
6	10	5.8	Ti	−0.5
			Cu	0
			Ag	1.1
			Pb	2.6

[a] A_F is the fragment mass used in the factorization analysis: $A_F=18-n-2$; i.e., for the case when two particles are emitted in the ablation stage.

TABLE XII. Values for $r(F,T)$ showing weak-factorization systematics.

	Target					
A_F	C	Al	Ti	Cu	Ag	Pb
15	1.064	1.032	1.012	1.005	0.989	0.973
13	0.993	0.996	0.999	0.999	1.001	1.003
10	0.898	0.948	0.980	0.992	1.017	1.043

The solid curves in Figs. 2(a) and (b) were derived using this assumption. (Note that these curves do not depend upon the value of r_0 used.) One can see that a deviation from weak factorization of this lesser magnitude is not ruled out by the data; but neither do the data exhibit the trend indicated by this assumption.

Bleszynski and Sander[11] suggested parametrizing the target dependence of fragmentation cross sections as

$$\sigma \propto (A_P^{1/2}+A_T^{1/3})^y , \tag{28}$$

where the exponent y indicates whether a process is peripheral, $y \approx 1$ (σ is proportional to the sum of the radii), or central, $y \approx 2$ (σ is proportional to the area which represents the total reaction cross section). They predicted (from abrasion-ablation calculations) that y depends upon the fragmentation channel and that it should increase from a value near unity for a single-nucleon removal process to a value approaching twice that for removing a significant number of nucleons from the projectile. Figure 3 shows the results of fitting the fragmentation cross sections with the functional form of Eq. (28), where a value of y is determined for each fragment and projectile (except that the EMD fragments are not included). The curve was obtained from the results of the abrasion-ablation calculations presented in Ref. 11. It can be seen in Fig. 3 that for a small number of nucleons removed ($A_P - A_F \leq 6$), the experimentally determined values for y do not cluster enough to rule out this model, but for lighter fragments ($A_P - A_F > 6$), the data deviate significantly from the trend of the model. One can also see, with this parametrization, that the data do not show the predicted dependence upon the fragmentation channel.

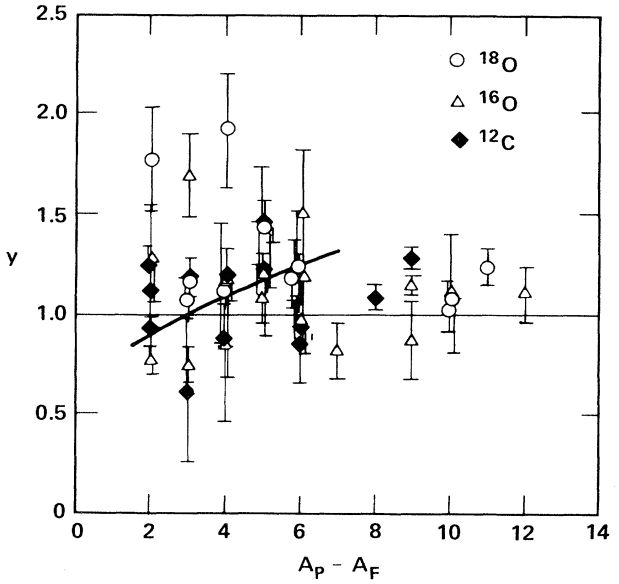

FIG. 3. Values of the exponent y vs $A_P - A_F$ for ^{18}O, ^{16}O, and ^{12}C projectiles (see the text for a discussion of the derivation of these values). The curve, obtained from the results of Ref. 11, shows the value of y expected from the abrasion-ablation theory.

IV. IMPLICATIONS

The present data indicate that strong factorization is probably violated. However, a comparison of the data for the projectiles ^{12}C, ^{16}O, ^{18}O, and ^{56}Fe shows that strong factorization certainly is not violated to the extent predicted by either the abrasion-ablation theory or our excitation-decay model. That this is the case indicates that the amount of overlap of the target and projectile nuclei, leading to peripheral fragmentation, actually is less than predicted by these models. In other words, peripheral fragmentation occurs at larger impact parameters than those predicted by the abrasion-ablation and our excitation decay models.

Of the fragmentation data sets that exist now, the one for ^{18}O projectiles[2] provides us with the most stringent test of weak factorization. It is clear, from the analysis described above, that the deviation from weak factorization predicted by the abrasion-ablation model is not manifested in any of the present data, especially those for ^{18}O projectiles. Moreover, the data (excluding hydrogen targets and fragments) show no systematic deviation whatever from weak factorization; there is no dependence of the target factor upon the fragmentation channel.

Within a geometrical picture of peripheral collisions, a deviation from weak factorization can result only when the branching to a fragmentation channel depends upon the amount of overlap of the target and projectile nuclei. It is clear from the results presented here that any dependence of the fragmentation channel upon impact parameter is much smaller than that predicted by the abrasion-ablation theory.

Thus, from the combined results of the strong- and weak-factorization analyses, we know that the average impact parameter leading to peripheral fragmentation is such that the target and projectile do not overlap very much and that the range of impact parameters leading to the various fragmentation channels is quite small.

The final conclusion we draw from this analysis is that peripheral fragmentation appears to be dominated by an excitation and decay process, in which weak factorization is exact, and that the abrasion process of the abrasion-ablation theory does not provide a valid description for the fragmentation process.

This work was performed under the auspices of the U.S. Department of Energy under Contract Nos. W-7405-ENG-48 (LLNL) and DE-AC03-76SF00098 (LBL) and the National Aeronautics and Space Administration under Grant No. NGR 05-003-513.

*Present address: Lawrence Berkeley Laboratory, Berkeley, CA 94720.

[1]P. J. Lindstrom, D. E. Greiner, H. H. Heckman, and Bruce Cork, Lawrence Berkeley Laboratory Report No. LBL-3650, 1975 (unpublished).

[2]D. L. Olson, B. L. Berman, D. E. Greiner, H. H. Heckman, P. J. Lindstrom, G. D. Westfall, and H. J. Crawford, Phys. Rev. C 24, 1529 (1981).

[3]G. D. Westfall, L. W. Wilson, P. J. Lindstrom, H. J. Crawford, D. E. Greiner, and H. H. Heckman, Phys. Rev. C 19, 1309 (1979).

[4]W. R. Frazer, L. Ingber, C. H. Mehta, C. H. Poon, D. Silverman, K. Stowe, P. D. Ting, and H. J. Yesian, Rev. Mod. Phys. 44, 284 (1972).

[5]J. Cugnon and R. Sartor, Phys. Rev. C 21, 2342 (1980).

[6]This is the case for ^{16}O projectiles striking C targets (Ref. 1) and for ^{18}O projectiles striking Al targets (Ref. 2).

[7]This is a simplification. The transition radius is a weighted average of the probability distribution (the transition density), and in general does not correspond to the distance for which the transition density is a maximum. For heavy ions, however, the data at present do not warrant this fine distinction.

[8]J. Hüfner, K. Schäfer, and B. Schürmann, Phys. Rev. C 12, 1888 (1975).

[9]J. D. Bowman, W. J. Swiatecki, and C. F. Tsang, Lawrence Berkeley Laboratory Report No. LBL-2908, 1973 (unpublished).

[10]R. J. Glauber, in *Lectures in Theoretical Physics,* edited by W. E. Brittin and L. G. Dunham (Interscience, New York, 1959), Vol. 1.

[11]M. Bleszynski and C. Sander, Nucl. Phys. A326, 525 (1979).

[12]P. J. Karol, Phys. Rev. C 11, 1203 (1975).

[13]R. Hofstadter and H. R. Collard, in *Landolt-Bornstein: Numerical Data and Functional Relationships in Science and Technology,* edited by H. Schopper (Springer, Berlin, 1967), Group I, Vol. 2, p. 21.